Abroad Predoctoral Research School Year Thesis Report

Gravity currents : Theoretical modelling and numerical analysis

Submitted for evaluation by
Wakim Arnold

External supervisors
Prof. Eckart Meiburg
Mohamad M. Nasr-Azadani

Internal supervisor
Prof. Rachid Bennacer

School-year 2014-2015

Contents

List of Figures

Acknowledgments

I would like to express my sincere gratitude to Prof. Eckart Meiburg for his bright and limpid monitoring and for his tremendous support.

I also want to thank Mohamad Nasr-Azadani for being the best tutor throughout this project. His enthusiasm and work have always spurred my approach and dedication to this project.

Finally; I would like to express my deep appreciation to Prof. Rachid Bennacer for encouraging me to undertake this project.

1 Introduction to gravity currents

1.1 Generalities and definitions

Gravity currents refer to flows in a gravitational field. Such flows are driven by a density difference where a denser fluid propagates through a lighter fluid, and the motion is therefore mainly in the horizontal direction. For example, pouring water on a plane forms a gravity current because of the density difference between water and air.

From pyroclastic flows to submarine avalanches, gravity currents occur in a wide variety of natural scenarii. Therefore it is essential to study such currents.

Gravity currents are driven by gravity. The difference in ρ between the fluids creates a pressure difference in the horizontal x-direction $\frac{\partial p}{\partial x} = \overrightarrow{grad}(p).\vec{e_x}$. The gravity effect associated with the density difference is referred to as the reduced gravity commonly g'.

Let ρ_c be the density of the current fluid, ρ_a the density of the ambient fluid and $\Delta\rho$ the density differece $\Delta\rho = \rho_c - \rho_a$. The reduced gravity is therefore defined as :

$$g' = \frac{|\Delta\rho|}{\max(\rho_a, \rho_c)}\ g$$

Usually ρ_c is greater than ρ_a thus $g' = \frac{|\Delta\rho|}{\max(\rho_a, \rho_c)}\ g = \frac{\rho_c - \rho_a}{\rho_c}\ g$

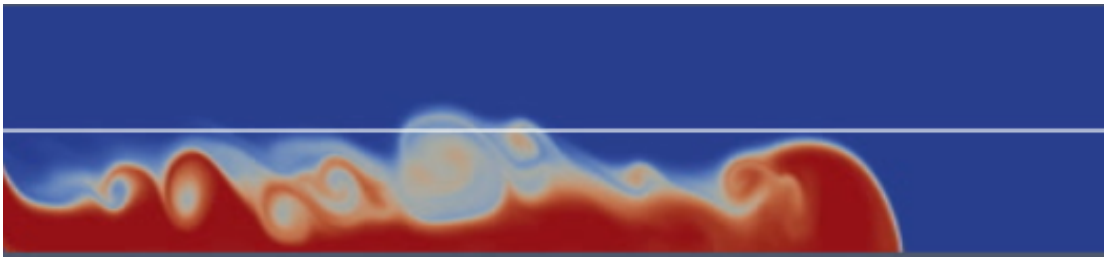

Figure 1.1: Gravity current propagating from left to right with $\rho_{red} > \rho_{blue}$

Theoretical modelling for gravity currents is possible through the use of approximations. The most common approximation for buoyancy driven flows is the Boussinesq approximation which is detailed in the following.

1.2 The Navier-Stokes equations

The governing equations for such flows are the Navier-Stokes equations for incompressible flow of Newtonian fluids.

The first, the mass continuity equation regardless of the flow assumptions. It describes the transport of a conserved quantity, in this case, it is mass.

$$\frac{\partial \rho}{\partial t} + \nabla(\rho \boldsymbol{v}) = 0$$

The general form Navier-Stokes momentum equations is:

$$\rho\left(\frac{\partial \boldsymbol{v}}{\partial t} + (\boldsymbol{v}\cdot\nabla)\,\boldsymbol{v}\right) = -\nabla p + \boldsymbol{f}_v + \rho\boldsymbol{g} + \mu\nabla^2\boldsymbol{v}$$

On the right-hand side of the momentum equations are the forces applied to the fluid. They belong to different categories :

- The internal forces : pressure and viscosity. The pressure exists even if the fluid is at rest, and is also called hydrostatic pressure.
  The viscosity of a fluid measures its resistance to gradual deformation by shear stress or tensile stress.
- The body forces such as gravity or Lorentz force in presence of magnetic field.
- Surface forces : most of the time they are due to boundary conditions.

In the Cartesian coordinate system the equations for an incompressible flow are :

$$\frac{\partial v_x}{\partial x} + \frac{\partial v_y}{\partial y} + \frac{\partial v_z}{\partial z} = 0$$

$$\rho\left(\frac{\partial v_x}{\partial t} + v_x\frac{\partial v_x}{\partial x} + v_y\frac{\partial v_x}{\partial y} + v_z\frac{\partial v_x}{\partial z}\right) = -\frac{\partial p}{\partial x} + \rho g_x + \mu\left(\frac{\partial^2 v_x}{\partial x^2} + \frac{\partial^2 v_x}{\partial y^2} + \frac{\partial^2 v_x}{\partial z^2}\right) + \rho f_{v_x}$$

$$\rho\left(\frac{\partial v_y}{\partial t} + v_x\frac{\partial v_y}{\partial x} + v_y\frac{\partial v_y}{\partial y} + v_z\frac{\partial v_y}{\partial z}\right) = -\frac{\partial p}{\partial y} + \rho g_y + \mu\left(\frac{\partial^2 v_y}{\partial x^2} + \frac{\partial^2 v_y}{\partial y^2} + \frac{\partial^2 v_y}{\partial z^2}\right) + \rho f_{v_y}$$

$$\rho\left(\frac{\partial v_z}{\partial t} + v_x\frac{\partial v_z}{\partial x} + v_y\frac{\partial v_z}{\partial y} + v_z\frac{\partial v_z}{\partial z}\right) = -\frac{\partial p}{\partial z} + \rho g_x + \mu\left(\frac{\partial^2 v_z}{\partial x^2} + \frac{\partial^2 v_z}{\partial y^2} + \frac{\partial^2 v_z}{\partial z^2}\right) + \rho f_{v_z}$$

To this day, solutions to the Navier-Stokes equations are yet not proven (existence, unicity), they are one of the most important open problems in mathematics.
Therefore, except for simple cases, numerical simulations are the only way to show the behavior of the flow.
Moreover, pressure is a difficult variable to manipulate. In two dimensions it is possible to eliminate pressure by taking the curl of the Navier-Stokes equations and at the expense of introducing the derivatives of velocity.

With such a nonlinear system of partial differential equations, assumptions and approximations about the flow and the use of the vorticity field may be needed, as it will be shown in the following section and chapters.

1.3 Boussinesq approximation

The Boussinesq approximation states that density differences are relatively small. In a two-fluid case it means that $\rho_c \approx \rho_a$. Roughly it means that the density difference between ρ_a and ρ_c is used in the buoyancy term of the momentum equation only. Boussinesq flows are common in nature, industry and the built environment.
This approximation is extremely accurate and makes the related mathematics and physics much easier to handle. Indeed their mathematical analysis, Navier-Stokes simulations and experimental realizations are simpler. Moreover their interpretation covers a broader range of boundary conditions.
Non-Boussinesq systems are still awaiting a comprehensive investigation.

The essential idea in the Boussinesq approximation is the elimination of the vertical coordinate from the flow equations which was first done by Joseph Boussinesq in 1871, to construct an approximate solution for the solitary wave (or wave of translation). Subsequently, in 1872, Boussinesq derived the equations known nowadays as the Boussinesq equations.

1.4 Vorticity

1.4.1 Definition

The vorticity is a pseudovector field that describes the local spinning motion of a continuum near a point i.e its tendancy to rotate.

Mathematically this vector field denoted $\boldsymbol{\omega}$ is defined as the curl (rotational) of the velocity field $\boldsymbol{v}$.

$$\boldsymbol{\omega} = \boldsymbol{\nabla} \times \boldsymbol{v}$$

In Cartesian coordinates : $\boldsymbol{\omega} = \left(\frac{\partial v_z}{\partial y} - \frac{\partial v_y}{\partial z},\ \frac{\partial v_x}{\partial z} - \frac{\partial v_z}{\partial x},\ \frac{\partial v_y}{\partial x} - \frac{\partial v_x}{\partial y}\right)$

Roughly, the vorticity tells how the velocity vector changes when one moves by an infinitesimal distance in a direction perpendicular to it.

1.4.2 Vorticity equation

Let's rewrite the Navier-Stokes momentum equations assuming that the gravity is the only body force.

$$\frac{\partial \boldsymbol{v}}{\partial t} + \boldsymbol{v} \cdot \nabla \boldsymbol{v} = -\frac{1}{\rho}\nabla\left(p + gz\right) + \nu \nabla^2 \boldsymbol{v}$$

By taking the curl of the Navier-Stokes equations.

$$\nabla \times \frac{\partial \boldsymbol{v}}{\partial t} + \nabla \times (\boldsymbol{v} \cdot \nabla \boldsymbol{v}) = -\nabla \times \left(\frac{1}{\rho}\nabla\left(p + gz\right)\right) + \nabla \times \left(\nu \nabla^2 \boldsymbol{v}\right)$$

With appropriate smoothness properties :

$$\nabla \times \frac{\partial \boldsymbol{v}}{\partial t} = \frac{\partial}{\partial t}\left(\nabla \times \boldsymbol{v}\right) = \frac{\partial \boldsymbol{\omega}}{\partial t}$$

In the same manner the last term on the right becomes

$$\nabla \times \left(\nu \nabla^2 \boldsymbol{v}\right) = \nu \nabla^2 \boldsymbol{\omega}$$

The gravity term is $-\nabla \times \nabla(gz) = 0$

Let's take a closer look to the following term :

$$-\nabla \times \left(\frac{1}{\rho}\nabla p\right) = -\frac{1}{\rho}\ \nabla \times \nabla p - \frac{1}{\rho^2}\nabla\rho \times \nabla p$$

The following theorem states that :

$$\forall \boldsymbol{X} \in \mathbb{R}^3\ ,\ \nabla \times \nabla \boldsymbol{X} = 0$$

Therefore the previous equality becomes :

$$-\nabla \times \left(\frac{1}{\rho}\nabla p\right) = -\frac{1}{\rho^2}\nabla\rho \times \nabla p$$

It is possible to show that we have the following result :

$$\nabla \times (\boldsymbol{v} \cdot \nabla \boldsymbol{v}) = \nabla \times \nabla \left(\frac{\boldsymbol{v}^2}{2}\right) - \nabla \times ((\nabla \times \boldsymbol{v}) \times \boldsymbol{v})$$

Using the theorem stated above :

$$\nabla \times (\boldsymbol{v} \cdot \nabla \boldsymbol{v}) = -\nabla \times ((\nabla \times \boldsymbol{v}) \times \boldsymbol{v})$$

Therefore the vorticity equation becomes :

$$\frac{\partial \boldsymbol{\omega}}{\partial t} = \nabla \times ((\nabla \times \boldsymbol{v}) \times \boldsymbol{v}) - \frac{1}{\rho^2}\nabla\rho \times \nabla p + \nu\nabla^2\boldsymbol{\omega}$$

This equation can still be modified. Indeed in the previous equation the first and seconds terms on the right hand side of the equation can be simplified for incompressible flows. Considering that gravity is in the $-y$ direction.

The vorticity equation is therefore.

$$\begin{aligned} &\frac{\partial \boldsymbol{\omega}}{\partial t} + \boldsymbol{v} \cdot \nabla \boldsymbol{\omega} = -g' \frac{\partial \rho^*}{\partial x} \boldsymbol{e_z} + \nu\nabla^2\boldsymbol{\omega} \\ &\textbf{where}\ \ \rho^* = \frac{\rho - \rho_a}{\rho_c - \rho_a} \end{aligned} \tag{1.1}$$

2 Circulation-based modelling for gravity currents

2.1 Circulation-based integration

If we take a closer look Eq. 1.1 we clearly notice that it is a diffusion equation.
This rules the diffusion of vorticity in a specific volume or surface.
It exactly means that the vorticity variation is generated by advection due to the velocity field, it is also due to the baroclinic term in the equation.
Using such an equation is convenient because of the way it can be integrated.

As it is above-mentioned equation 1.1 is a diffusion equation that can be integrated over a control volume or a control surface.

For the following, all the cases are going to be studied in steady-state i.e $\dfrac{\partial \omega}{\partial t} = 0$.
Equation 1.1 therefore becomes :

$$\begin{aligned} &\boldsymbol{v} \cdot \boldsymbol{\nabla}\omega = -g' \frac{\partial \rho^*}{\partial x} + \nu \boldsymbol{\nabla}^2 \omega \\ &\textbf{where} \;\; \rho^* = \frac{\rho - \rho_a}{\rho_c - \rho_a} \end{aligned} \tag{2.1}$$

Let's integrate equation 2.1 over control surface called $\mathcal{A}$.

$$\iint_{\mathcal{A}} \boldsymbol{v} \cdot \boldsymbol{\nabla}\omega \; \mathrm{d}A \;=\; \iint_{\mathcal{A}} -g' \frac{\partial \rho^*}{\partial x} \; \mathrm{d}A \;+ \iint_{\mathcal{A}} \nu \boldsymbol{\nabla}^2 \omega \; \mathrm{d}A \tag{2.2}$$

Now, the divergence theorem states that :

$$\iint_{\mathcal{A}} \nu \boldsymbol{\nabla}^2 \omega \; \mathrm{d}A \;= \oint_{\Gamma} \nu \; \boldsymbol{\nabla}\omega \cdot \boldsymbol{n} \; \mathrm{d}\Gamma$$

For any scalar field g and any vector field $\boldsymbol{F}$, the divergence theorem leads to :

$$\iint_{\mathcal{A}} \left(\boldsymbol{F} \cdot \boldsymbol{\nabla} g + g \left(\boldsymbol{\nabla} \cdot \boldsymbol{F}\right)\right) \mathrm{d}A = \oint_{\Gamma} g\boldsymbol{F} \; \mathrm{d}\Gamma$$

Now by substituting $g \;= \omega$ and $\boldsymbol{F} \;= \boldsymbol{v}$ and using the incompressible flow assumption $\boldsymbol{\nabla} \cdot \boldsymbol{v} \;=\; 0$ the first term of equation 2.2 becomes :

$$\iint_{\mathcal{A}} \boldsymbol{v} \cdot \boldsymbol{\nabla}\omega \; \mathrm{d}A \;= \oint_{\Gamma} \omega \boldsymbol{v} \cdot \boldsymbol{n} \; \mathrm{d}\Gamma$$

So equation 2.2 turns into :

$$\oint_{\Gamma} \omega \boldsymbol{v} \cdot \boldsymbol{n} \, \mathrm{d}\Gamma = \iint_{\mathcal{A}} -g' \frac{\partial \rho^*}{\partial x} \, \mathrm{d}A \; + \oint_{\Gamma} \nu \, \boldsymbol{\nabla}\omega \cdot \boldsymbol{n} \, \mathrm{d}\Gamma \tag{2.3}$$

Equation 2.3 therefore states that the rate at which vorticity is convected out of the control volume at the downstream boundary equals the rate at which it is convected into the control volume at the upstream boundary, plus the rate at which it is generated inside the control volume as a result of baroclinic vorticity production.

This approach has advantadge of removing the pressure variable from the analysis. If information about the pressure is needed, we can solve the $x-$momentum equation at a later stage.
Indeed the vorticity-based modelling approach does not require the use of Bernoulli's principle nor the use of empirical energy assumption.
In the following, the Reynolds number will be sufficiently high $Re \geq 250$ as shown by M.M. Nasr-Azadani and E. Meiburg [6] so the viscous term can be neglected in the remaining.

2.2 Application : Gravity current propagating into shear

2.2.1 Formulation of the problem

In order to understand the use of the circulation based modelling for gravity current, the following example will deal with a gravity current propagating into shear. Evaluating the front velocity of a gravity current was a task that many scientist investigated (cf. Von Karman [2] & Benjamin [3]). Indeed knowing this velocity may be helpful when it comes to sizing immersed infrastructures to prevent them from being destroyed by gravity currents, etc. Let us consider a gravity current flowing from right to left with an unknown front velocity U_g, as described in Fig 2.1.

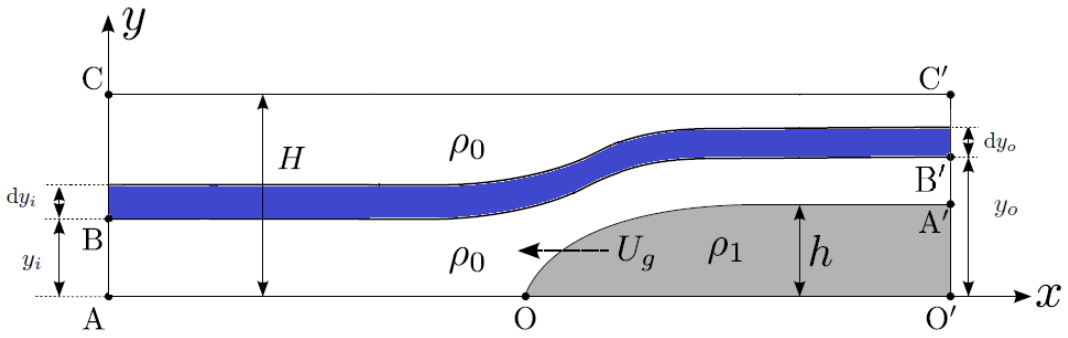

Figure 2.1: Gravity current propagating from right to left with a front velocity U_g

The equation of continuity along the streamline tube provide the following equation

$$u_i \mathrm{d}y_i = u_o \mathrm{d}y_o \tag{2.4}$$

Now, the conservation of vorticity along the streamline tube provide

$$-u_o \omega_o \mathrm{d}y_o - (-u_i \omega_i \mathrm{d}y_i) = -g' \frac{\Delta\rho}{\rho_c - \rho_a} (y_0 - y_i)$$

Therefore we obtain

$$u_i \omega_i \mathrm{d}y_i - u_o \omega_o \mathrm{d}y_o = -g' \frac{\Delta\rho}{\rho_c - \rho_a} (y_0 - y_i)$$

Using the relation $\Delta\rho = \dfrac{\mathrm{d}\rho_i}{\mathrm{d}y_i}\,\mathrm{d}y_i$ we can modify the conservation of vorticity

$$u_i\omega_i \mathrm{d}y_i - u_o\omega_o \mathrm{d}y_o = -g' \frac{\dfrac{\mathrm{d}\rho_i}{\mathrm{d}y_i}\mathrm{d}y_i}{\rho_c - \rho_a}\,(y_0 - y_i) \tag{2.5}$$

Now let us define the following substitution

$$\begin{cases} y_0 = y_i + \xi(y_i), \text{ therefore} \\ \mathrm{d}y_0 = \mathrm{d}y_i + \xi'(y_i)\mathrm{d}y_i \text{ where } \xi'(y_i) = \dfrac{\mathrm{d}\xi}{\mathrm{d}y_i} \end{cases} \tag{2.6}$$

Hence we can have $\dfrac{\mathrm{d}y_0}{\mathrm{d}y_i} = 1 + \xi'$

Using equation 2.4 we notice that

$$u_0(y_0) = u_i(y_i)\left(\frac{\mathrm{d}y_0}{\mathrm{d}y_i}\right)^{-1} = \frac{u_i(y_i)}{1 + \xi'(y_i)} \tag{2.7}$$

Now let us compute $\omega_0(y_0)$ using the definition of $\omega = -\dfrac{\mathrm{d}u}{\mathrm{d}y}$. Therefore we have

$$\omega_0(y_0) = -\frac{\mathrm{d}u_0}{\mathrm{d}y_0} = \frac{\mathrm{d}u_0}{\mathrm{d}y_i}\frac{\mathrm{d}y_i}{\mathrm{d}y_0} = -\frac{1}{1+\xi'}\frac{\mathrm{d}u_0}{\mathrm{d}y_i} \tag{2.8}$$

Notice that we know $u_0(y_0) = u_i(y_i)\dfrac{1}{1+\xi'}$, therefore $\omega_0(y_0) = -\dfrac{1}{1+\xi'}\dfrac{\mathrm{d}}{\mathrm{d}y_i}\left(\dfrac{u_i}{1+\xi'}\right) = -\dfrac{1}{1+\xi'}\dfrac{\dfrac{\mathrm{d}u_i}{\mathrm{d}y_i}(1+\xi') - \xi'' u_i(y_i)}{(1+\xi')^2}$

such that $\omega_0(y_0) = -\dfrac{1}{(1+\xi')^3}\left[\dfrac{\mathrm{d}u_i}{\mathrm{d}y_i}(1+\xi') - \xi'' u_i(y_i)\right]$

Now replacing ω_0 in equation 2.5 we obtain the following non-linear ODE

$$\xi'' u(y_i) + u_i'(y_i)\left[(1+\xi')^3 - (1+\xi')\right] - (1+\xi')^3\left[\xi\frac{g'\rho_i'}{u_i(y_i)\,(\rho_c - \rho_a)}\right] = 0 \tag{2.9}$$

Now, let us take a look at the boundary conditions. It is important to note that it is a second order non-linear ODE, therefore we need two boundary conditions.

We have $\boxed{\xi(y_i = 0) = h \ (AOA) \ and \ \xi(y_i = H) = 0 \ (BB')}$.

In order to determine ξ we still need a condition on its first derivative. Indeed, the vorticity conservation across the interface (OA) gives $\dfrac{U_0^2(h)}{2} = g'h\dfrac{\rho_c - \rho_i(0)}{\rho_c - \rho_a}$.

Using equation 2.7 we notice that $u_0(h) = \dfrac{u_i(y_i = 0)}{1 + \xi'(y_i = 0)}$

$\xi'(y_i = 0) = \dfrac{u_i(y_i = 0)}{u_0(h)} - 1$

Note that we have three boundary conditions while we only need two. One of them will allow us to determine U_g the velocity of the gravity current.
Therefore we have the following Cauchy problem.

$$\begin{cases} \xi''u(y_i) + u_i'(y_i)\left[(1+\xi')^3 - (1+\xi')\right] - (1+\xi')^3\left[\xi\dfrac{g'\rho_i'}{u_i(y_i)\,(\rho_c-\rho_a)}\right] = 0 \\ \xi(y_i=0) = h \ (AOA) \ and \ \xi(y_i=H) = 0 \ (BB') \\ \xi'(y_i=0) = \dfrac{u_i(y_i=0)}{u_0(h)} - 1 \end{cases} \tag{2.10}$$

2.2.2 Numerical Solution to determine U_g

The Cauchy problem 2.10 is non-linear and cannot be solve with an analytical solution. Hence, the use of an algorithm is the only way to approach the value of U_g* to respect the boundary conditions.

With MATLAB it is possible to solve Ordinary Differential Equations (ODEs) using the function *ODE45* function.
As it above-mentionned U_g is the unknown to be determined but to solve the problem U_g is needed.
The following algorithm is similar to a **do while** loop in C++.
The procedure has to be started with an initial "guess" of U_g and while the condition $\xi(y_i = H) = 0$ is not satisfied then it will change the initial guess.

Indeed if $\xi(y_i = H) > 0$, it means that the slope at $y_i = 0$, which is nothing but U_g, is too important so it has to be reduced. $\xi(y_i = H) < 0$, it means that the slope at $y_i = 0$ is too low so it has to be increased.

The following procedure has been written with dimensionless equations and in the case where ρ_i is uniform which means $\rho_i' = 0$. The velocity profile is linear and its expression is $u(y) = U_g + \frac{1}{2}\Delta U(1-2y)$
We consider a layer height of $h = 0.2$ and a total height (control volume) $H = 1$

Listing 2.1: sample code

```
% PROCEDURE TO FIND Ug

Ug = 0.7;  % Arbitrary choice of Ug
DeltaU = 0.4;  % We choose Delta U however we want for the linear profile
h=0.2; % Current height, it doesn't matter how it is chosen.
H=1;


range_for_y = [0 1.];    % Interval of solving for the ODE
A=(Ug+(DeltaU/2))/sqrt(2*h/H) - 1; %  value of Zeta'(0)
initial = [ h/H ; A];

velocity = @(t)(Ug+0.5*DeltaU*(1-2*t)); % Wanted profile. Can be anything.

equationfunction = @(t,y)[ y(2) ; -1/(velocity(t))*(-DeltaU)*((1+ y(2))^3 -(1 + y
    (2)))  ]; % solving for the first time


[t,y] = ode45(equationfunction, range_for_y, initial);

T=size(t);
```

```
T(1);

error = y(T(1));

n=3;
eps = 10^(-n);

iter =0;

% Now it's important to understand the 'trick'. We want to find the Ug to
% respect Zeta(1)=0. So what we do is : 1) We solve the equation for
% the 1st time. Then we see wether Zeta(1) < 0 (close to 0) or > 0 (close to 0).
% If Zeta(1) < 0 it means that the slope in y = 0 (A = Zeta'(0)) was not
% big enough so we decrease its value by 0.001. And we check wether
% Zeta(1) < 0 (close to 0) or > 0 (close to 0). Now if Zeta(1) > 0 it means that
% the slope in y = 0 (A = Zeta'(0)) was already
% big enough so we decrease its value by 0.001.
% The while loop may not converge so we can add a condition for the loop to
% stop, like adding a counter called iter.

while abs(error) > eps && iter < 1000
   if  y(T(1)) > 0
       Ug = Ug - 0.001;
       A=(Ug+(DeltaU/2))/sqrt(2*h/H) - 1; % value of Zeta'(0)
       initial = [ h/H ; A];
       velocity = @(t)(Ug+0.5*DeltaU*(1-2*t));
       equationfunction = @(t,y)[ y(2) ; -1/(velocity(t))*(-DeltaU)*((1+ y(2))^3
           -(1 + y(2)))  ];
       [t,y] = ode45(equationfunction, range_for_y, initial);
       T=size(t);
       error = y(T(1));
   else y(T(1)) < 0
       Ug = Ug + 0.001;
       A=(Ug+(DeltaU/2))/sqrt(2*h/H) - 1; %  value of Zeta'(0)
       initial = [ h/H ; A];
       velocity = @(t)(Ug+0.5*DeltaU*(1-2*t));
       equationfunction = @(t,y)[ y(2) ; -1/(velocity(t))*(-DeltaU)*((1+ y(2))^3
           -(1 + y(2)))  ];
       [t,y] = ode45(equationfunction, range_for_y, initial);
       T=size(t);
       error = y(T(1));
   end
   iter = iter+1;
end

Ug
y(T(1))
iter

plot(t,y(:,1))
xlabel('y*');
ylabel('Xi');
s1 ='Ug =  ';
s3 = num2str(Ug);
s = strcat(s1,32,s3);
legend(s);
title('Numerical solution of the ODE & U_{g}')
```

The computed solution $\xi(y)$ which respects the boundary conditions leads to the value $U_g^* = 0.378$ as shown in Fig 2.2.

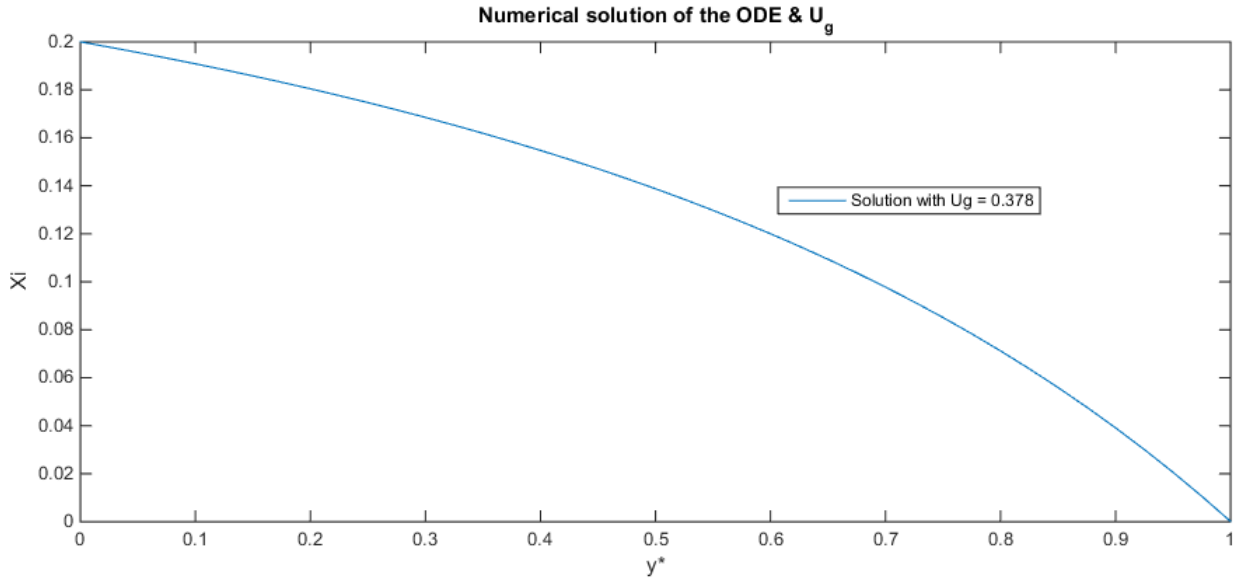

Figure 2.2: Numerical solution of the ODE to obtain U_g

This application helps understanding the circulation-based modelling for gravity currents. The main study detailled in the next chapter deals with gravity currents propagating over complex topography.

3 Gravity Currents Propagating over Complex Topography

Understanding and modelling gravity currents flowing over a complex topography is a subject that has been investigated by Long, Houghton & Kasahara and Baines & Davies.

3.1 Two-layer flow over streamlined obstacle

The following study deals with a stratified fluid flowing over a streamlined obstacle. Let us consider a two-layer flow such as index $_1$ refers to the lower layer (denser fluid) and index $_2$ refers to the upper layer (lighter fluid) cf. figure 3.1. Both fluids are flowing from left to right at the initial velocity u_0.

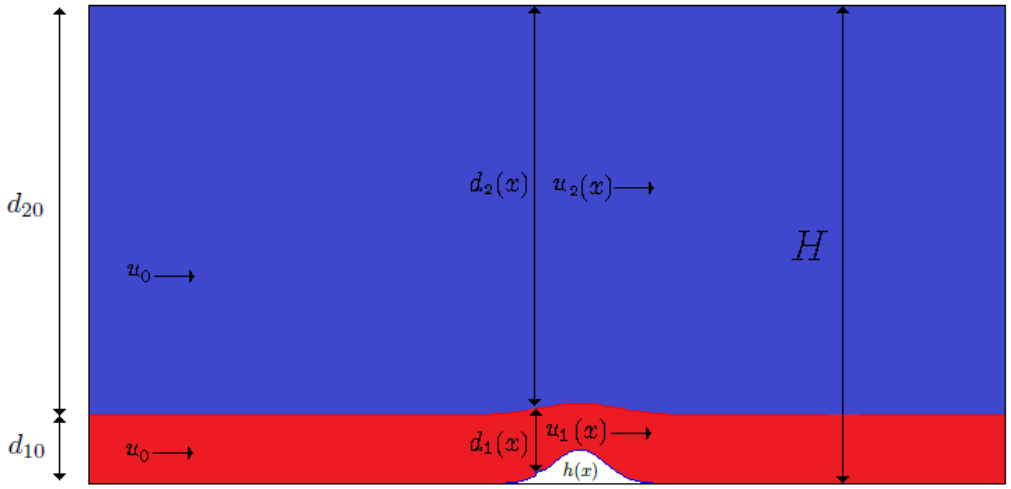

Figure 3.1: Stratified fluid, $\rho_2 < \rho_1$ flowing over a streamlined obstacle with the inflow velocity u_0 in the channel height H.

From experiments led by R. Long [4], four types of flows have been observed.
The lower layer fluid may flow over the topography to lead to a flow without blocking. When the right conditions are gathered, the lower layer may rise or dip over the crest of the obstacle, which would lead to, respectively, a supercritical or subcritical regime.
When the conditions are not gathered, the obstacle may partially or completely block the lower layer fluid.
The goal of the following sections is to determine the conditions for the lower layer fluid to flow over the topgraphy or become partially or completely blocked.

For a matter of convenience, the topography will be a smooth gaussian obstacle.

3.2 Flow without blocking

In this section, all notations refer to figure 3.1.

3.2.1 Flow Without Blocking - Theory

Mass conservation leads to equations 3.1 and 3.2.

$$u_1(x)d_1(x) = u_0 d_{10} \tag{3.1}$$

$$u_2(x)d_2(x) = u_0 d_{20} \tag{3.2}$$

Considering a location x where $h(x) \neq 0$, the geometry provides equation 3.3

$$d_1(x) + d_2(x) + h(x) = H \tag{3.3}$$

At the interface between the lower and upper layers, the vorticity may be expressed as :

$$\frac{(u_2 - u_1)(u_2 + u_1)}{2} = g'(d_{20} - d_2) = \frac{1}{2}(u_2^2 - u_1^2) \tag{3.4}$$

From equation 3.1, equation 3.2 and equation 3.3 we can make the following substitutions :

$$u_1(x) = \frac{u_0 d_{10}}{d_1(x)} \; and \; u_2(x) = \frac{u_0 d_{20}}{d_2(x)} = \frac{u_0 d_{20}}{H - h(x) - d_1(x)}$$

If we substitute the previous formulae in Eq 3.4 and make the equation dimensionless, we get :

$$\frac{\left(\frac{d_{20}}{d_{10}}\right)^2 F^2}{\left(1 + \frac{d_{20}}{d_{10}} + \frac{h(x)}{d_{10}} - \frac{d_1(x)}{d_{10}}\right)^2} - \frac{F^2}{\left(\frac{d_1(x)}{d_{10}}\right)^2} = 2\left(\frac{d_1(x)}{d_{10}} + \frac{h(x)}{d_{10}} - 1\right) \; where \; F = \frac{u_0}{\sqrt{g' d_{10}}} \tag{3.5}$$

For an infinitely deep upper layer $\frac{d_{20}}{d_{10}} \longrightarrow +\infty$, the first term in Eq 3.5 becomes F^2
Therefore, we obtain the third degree equation where $d_1(x)$ is the unknown :

$$\begin{gathered} d_1^*(x)^3 + \left(D_0(x) - 1 - \frac{F^2}{2}\right) d_1^*(x)^2 + \frac{F^2}{2} = 0 \\ where \; d_1^*(x) = \frac{d_1(x)}{d_{10}} \; and \; D_0(x) = \frac{h(x)}{d_{10}} \end{gathered} \tag{3.6}$$

Eq 3.6 is a third degree polynomial, let's subsitute $d_1(x)$ by X to avoid all confusion.

For third degree equations there are analytical solutions. Also, it is possible to find a critical line as a function of $D_0(x)$ and F, to know wether solution are real or complex.
The method of resolution is the **Cardano-Tartaglia Method for third degree equations.**

Equation 3.6 becomes :

$$X^3 + \left(D_0 - 1 - \frac{F^2}{2}\right) X^2 + \frac{F^2}{2} = 0$$

By using the change of variable $X = z - \frac{1}{3}\left(D_0 - 1 - \frac{F^2}{2}\right)$ equation 3.6 becomes :

$$\begin{aligned} & z^3 + pz + q = 0 \\ & \textit{where } p = -\frac{1}{3}\left(D_0 - 1 - \frac{F^2}{2}\right)^2 \\ & \textit{and } \ q = \frac{2}{27}\left(D_0 - 1 - \frac{F^2}{2}\right)^3 + \frac{F^2}{2} \end{aligned}$$

Let's substitute $z = u + v$ thus :

$$\begin{aligned} & u^3 + 3u^2v + 3uv^2 + v^3 + p(u+v) + q = 0 \\ & \textit{therefore } u^3 + v^3 + (3uv + p)(u+v) + q = 0 \end{aligned}$$

With the simplification condition $3uv + p = 0$, the previous implies the following system :

$$\begin{cases} u^3 + v^3 = -q \\ u^3 v^3 = -\dfrac{p^3}{27} \end{cases}$$

Thus u^3 and v^3 are solutions of the second degree equation $Y^2 + qY - \frac{p^3}{27} = 0$
The discriminant denoted δ and is by the formula $\delta = q^2 + \frac{4}{27}p^3$

$$\begin{aligned} \delta &= \left[\frac{2}{27}\left(D_0 - 1 - \frac{F^2}{2}\right)^3 + \frac{F^2}{2}\right]^2 - \frac{4}{27}\left[\frac{1}{3}\left(D_0 - 1 - \frac{F^2}{2}\right)^2\right]^3 \\ \delta &= \frac{4}{27}\left(D_0 - 1 - \frac{F^2}{2}\right)^6 + \frac{2F^2}{27}\left[D_0 - 1 - \frac{F^2}{2}\right]^3 + \frac{F^4}{4} - \frac{4}{27^2}\left(D_0 - 1 - \frac{F^2}{2}\right)^6 \\ \delta &= \frac{F^4}{4} + \frac{2F^2}{27}\left[D_0 - 1 - \frac{F^2}{2}\right]^3 \\ \delta &= F^2\left\{\frac{F^2}{4} + \frac{2}{27}\left[D_0 - 1 - \frac{F^2}{2}\right]^3\right\} \end{aligned}$$

When $\delta < 0$ there are three real solutions.
When $\delta = 0$ there are three real solutions and two of these are equal.
When $\delta > 0$ there are three solution one is real and two are complex conjugate but this case is physically not meaningful cf. section 3.3 .

The critical curve (cf. figure 3.2) which separates physically meaningful and meaningless solutions is obtained when $\delta = 0$. Thus comes the following equation:

$$D_0 = 1 - \frac{3}{2}\sqrt[3]{F^2} + \frac{F^2}{2} \tag{3.7}$$

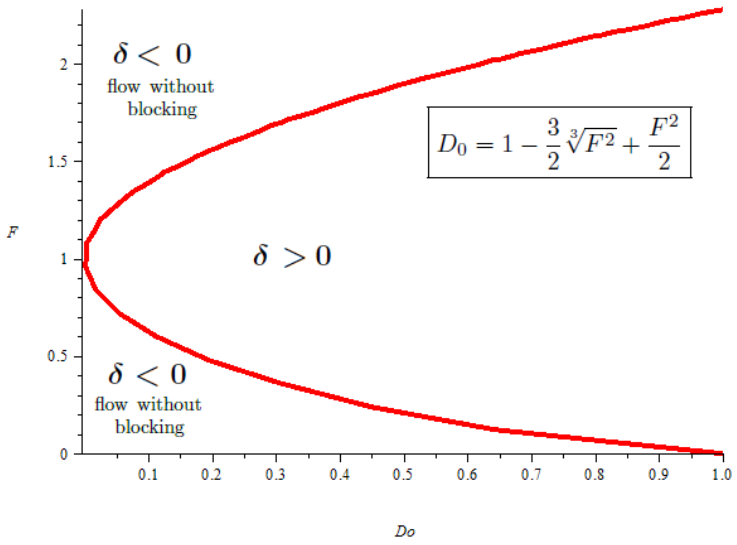

Figure 3.2: Critical curve in the plane (D_0, F)

This critical curve has been found by R.R. Long [4] in 1954, using Bernoulli's equation and hydrostatic pressure assumptions, and has also been found by Houghton & Kasahara [5] in 1967 using the steady state shallow water equations.
Figure 3.2 show the regions where the flow without blocking occurs.
When $\delta > 0$, the previous theoretical modelling leads to non-meaningful physical solutions. Indeed, from experiments by R.R. Long [4], hydraulic jumps are observed, hence the previous modelling is obsolete when $\delta > 0$, section 3.3 investigates the previous phenomena.

3.2.2 Solutions for $\delta = 0$ over the crest

In this case it is only possible to express the theoretical solution above the obstacle crest. Indeed if x_{bump} denotes the location of the crest then for $x \leq x_b$ if $D_0(x) > 1 - \frac{3}{2}\sqrt[3]{F^2} + \frac{F^2}{2}$ hydraulic jumps will appear. Let us assume that $D_0(x) < 1 - \frac{3}{2}\sqrt[3]{F^2} + \frac{F^2}{2}$ for $x < x_b$ and $D_0(x_b) = 1 - \frac{3}{2}\sqrt[3]{F^2} + \frac{F^2}{2}$.
Hence the solutions $z_0,\ z_1,\ z_2$ are :

$$z_0 = 2\sqrt[3]{\frac{-q}{2}} = \frac{3q}{p} \quad and \quad z_1 = z_2 = -\sqrt[3]{\frac{-q}{2}} = -\frac{3q}{2p}$$

Therefore $p = -\frac{3F^{\frac{4}{3}}}{4}$ and $q = \frac{F^2}{4}$

Consequently the solutions become :

$$z_0 = -F^{\frac{2}{3}} \quad and \quad z_1 = z_2 = \frac{1}{2}F^{\frac{2}{3}}$$

Thus the solutions for the layer height above the obstacle crest are :

$$d_1^*(x_b)_0 = z_0 - \frac{1}{3}\left(D_0 - 1 - \frac{F^2}{2}\right) = -\frac{3}{2}F^{\frac{2}{3}} \quad and \quad d_1^*(x_b)_1 = d_1^*(x_b)_2 = F^{\frac{2}{3}}$$

Only the positive solution is physically meaningful. Numerical simulations to verify these results are delicate, since (D_0, F) is on the critical curve.

3.2.3 Solutions for $\delta < 0$

To obtain the solution it is necessary to use complex notation to obtain solution in $\mathbb{R}$. The solutions can be expressed as follows :

$$z_k = 2\sqrt{\frac{-p}{3}}\cos\left(\frac{1}{3}\arccos\left(\frac{-q}{2}\sqrt{\frac{27}{-p^3}}\right)+\frac{2k\pi}{3}\right) \qquad \text{where} \qquad k \in \{0,1,2\}$$

The previous leads to :

$$d_1(x) = \frac{d_{10}}{3}\left[D_0(x) - 1 - \frac{F^2}{2}\right]\left[2\cos\left(\frac{1}{3}\arccos\left\{-\frac{27F^2}{4\left[D_0(x)-1-\frac{F^2}{2}\right]^3}-1\right\}+\frac{2k\pi}{3}\right)-1\right] \tag{3.8}$$

The exact solution to the physical problem with boundary condition $d(x=0) = d_{10}$ depends on k.
When $F < 1$, $k = 1$ gives the correct solution for a subcritical regime cf. figure 3.3 whereas $k = 2$ gives the correct solution when $F > 1$ cf. figure 3.4

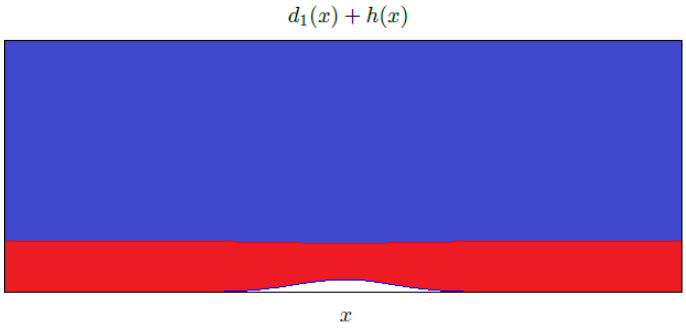

Figure 3.3: $d_1(x) + h(x)$ for $F = 0.3$, $D_0 = 0.25$ for $d_{10} = 1$ $k = 1$. As expected the denser fluid dips over the crest since $F < 1$. The dip is fairly small depending on were the point (D_0, F) in the region $\delta < 0 \cap F < 1$

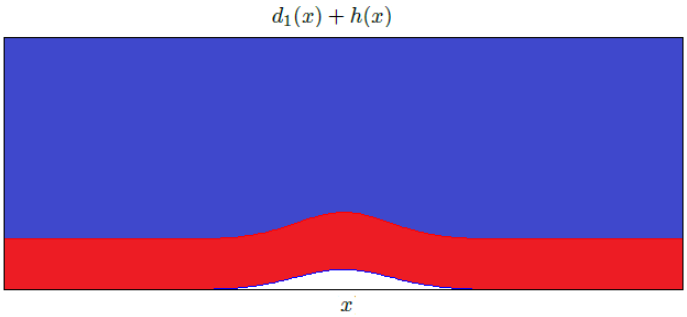

Figure 3.4: $d_1(x) + h(x)$ for $F = 2.2$, $D_0 = 0.4$ for $d_{10} = 1$ $k = 2$. The denser fluid rises over the crest since $F > 1$.

3.2.4 Flow without blocking - Direct Numerical Simulation

To validate theoretical results on flow without blocking, we use Direct Numerical Simulations (DNS) with TURBINS [1] (M.M. Nasr-Azadani E. Meiburg) which is an immersed boundary, Navier - Stokes code for the simulation of gravity and turbidity currents interacting with complex topographies.
For this configuration the non-parallel version TURBINS2D is used.

DNS for the supercritical case

For the supercritical case, the point selected in figure 3.2 is $(D_0, F) = (0.4, 2)$. Figure 3.5 is a snapshot[1] of the DNS when steady state is reached, as previously mentionned a rise above the crest is observed.

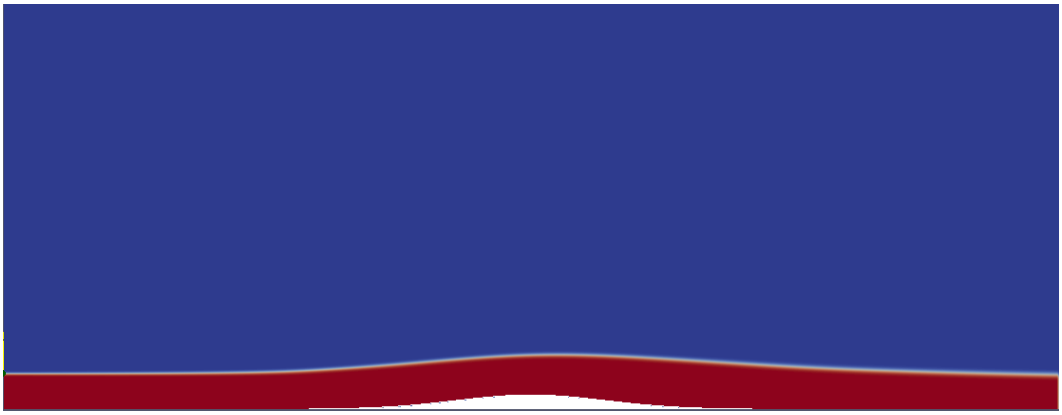

Figure 3.5: Snapshot of the DNS where the red layer represent $d_1(x)$ for $F = 2$, $D_0 = 0.4$.

The post-processing of the data allows the plotting on figure 3.6 $[d_1(x) + h(x)]_{DNS}$ and $[d_1(x) + h(x)]_{analytical}$

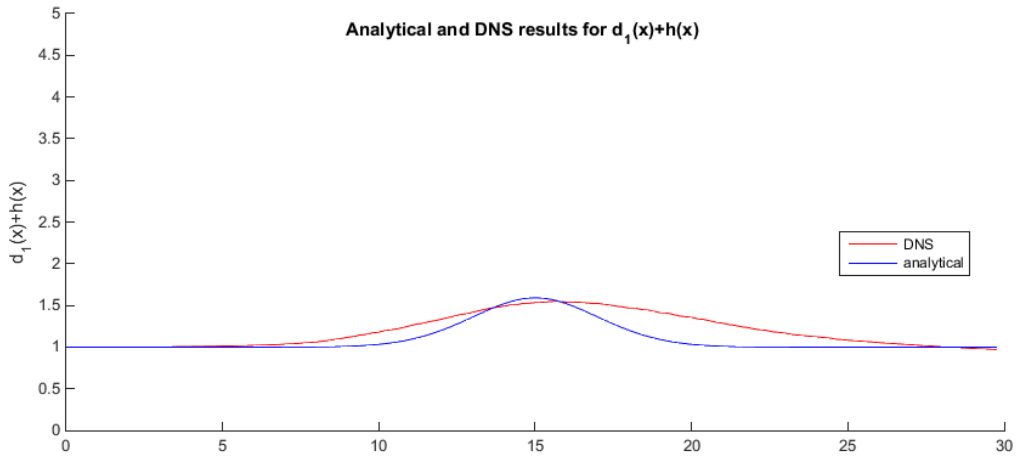

Figure 3.6: Post-processed data from the DNS. $[d_1(x) + h(x)]_{DNS}$ in red and $[d_1(x) + h(x)]_{analytical}$ in blue are plotted.

[1] Using paraview

In figure 3.7 the relative uncertainty $\Delta_{[d_1(x)+h(x)]} = \left| \frac{[d_1(x)+h(x)]_{analytical} - [d_1(x)+h(x)]_{DNS}}{[d_1(x)+h(x)]_{analytical}} \right|$ shows a 30% error between the theoretical model and the DNS, it is mainly due to the no-slip condition imposed on the topography.

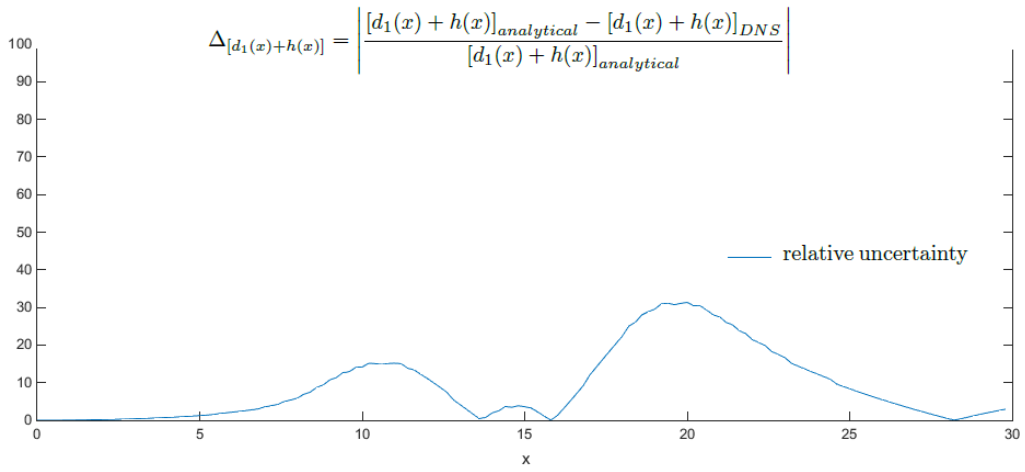

Figure 3.7: Relative uncertainty $\Delta_{[d_1(x)+h(x)]} = \left| \frac{[d_1(x)+h(x)]_{analytical} - [d_1(x)+h(x)]_{DNS}}{[d_1(x)+h(x)]_{analytical}} \right|$

The free-slip condition imposed on the obstacle allows the separation of the fluid. In figure 3.8 is the velocity streamlines show a recirculation bubble between the fluid and the obstacle.

Figure 3.8: Snapshot of the velocity streamlines from the DNS showing a recirculation bubble in blue between the fluid and the obstacle.

Nevertheless, the rise over the obstacle is observed and the value $d_1(x_b) + h(x_b)$ is accurate since $\Delta_{[d_1(x_b)+h(x_b)]} = 3.87\%$.

DNS for the subcritical case

The previous DNS domain is used for the subcritical case. For this DNS, $(D_0, F) = (0.25, 03)$. Once the steady state is reached, cf. figure 3.9, it is possible to compare the DNS with the analytical value for $d_1(x) + h(x)$.
In the subcritical region, we notice that $d_1(x)$ gets thinner in the obstacle area and a right-shift is still observed due to the free-slipping condition imposed on the topography. Figure 3.10 compare $[d_1(x) + h(x)]_{DNS}$ in and $[d_1(x) + h(x)]_{analytical}$.
In figure 3.11 the relative untertainty is such as $\Delta_{[d_1(x)+h(x)]} \leq 8\%$ across the channel, hence there is a good agreement between the model and the DNS.

Despite the maximum 30% difference for the supercritical case, the theoretical model agrees well with simulations.

Figure 3.9: Snapshot of the DNS for $F = 0.3$, $D_0 = 0.025$.

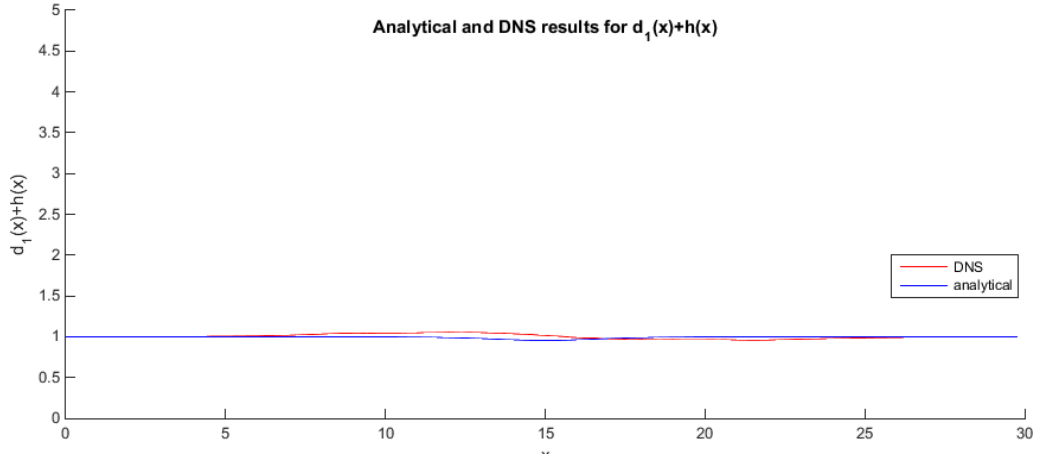

Figure 3.10: Post-processed data from the DNS. $[d_1(x) + h(x)]_{DNS}$ in red and $[d_1(x) + h(x)]_{analytical}$ in blue are plotted.

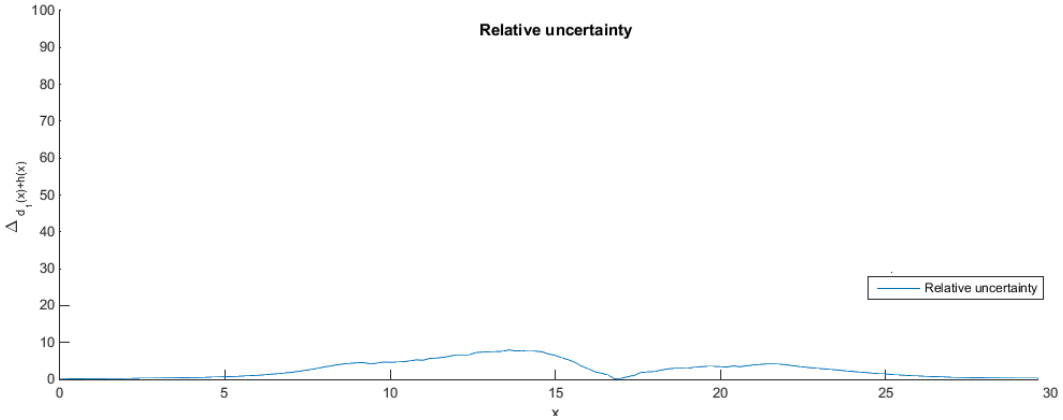

Figure 3.11: Relative uncertainty $\Delta_{[d_1(x)+h(x)]} = \left| \dfrac{[d_1(x) + h(x)]_{analytical} - [d_1(x) + h(x)]_{DNS}}{[d_1(x) + h(x)]_{analytical}} \right|$

3.3 Partial Blocking

Experimentally, Long [4] has shown that hydraulic jumps might happen and propagate upstream. These hydraulic jumps or bores appear because $\delta > 0$ cf. figure 3.2. Indeed, when the obstacle is high enough or the inlet Froude number is not enough, it means that at some point x^* on the obstacle, the following relation is verified at x^* : $D_0(x^*) = 1 - \frac{3}{2}\sqrt[3]{F^2} + \frac{F^2}{2}$. Hence, discontinuites appear and form the bores.

This section will focus on modelling bores propagating upstream and their velocity, assuming that the state is steady; this assumption will be verified and criticized further in the section with DNS.

3.3.1 Theoretical modelling for partial blocking

The following figure REFERENCE FIGURE will introduce the new variables for the theoretical modelling.

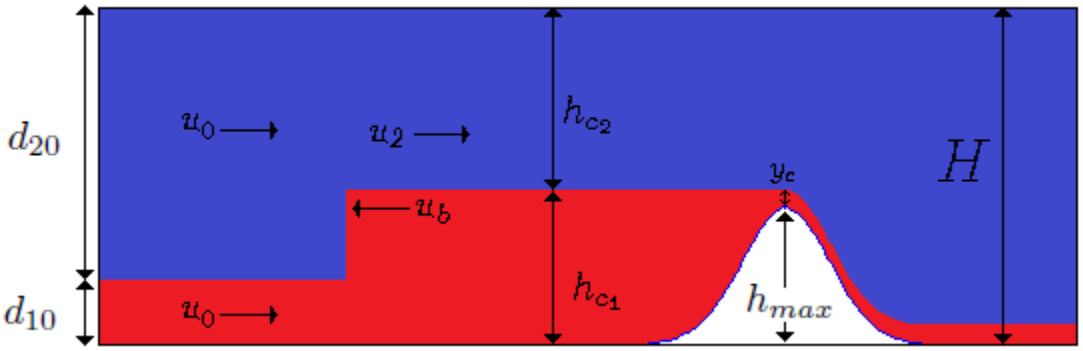

Figure 3.12: Bore propagating upstream after partial blocking by the obstacle.

Let us note that in this case, 5 unknowns are present, **since the upper layer is infinitely deep** :

- u_b the velocity of the bore propagating upstream in this case $u_b > 0$.
- h_b the bore height.
- u_{inb} the velocity inside the bore.
- y_c the layer height over the crest.
- u_c the fluid velocity over the crest.

In the reference frame moving with the upstream propagating bore, it is possible to establish 4 equations.

Between points A and B on figure REFERENCE FIGURE) mass conservation and the circulation equation provide :

$$(u + u_b)\, d_{10} = (u_{inb} + u_b)\, h_b \tag{3.9}$$

$$g'\,(h_b - d_{10}) = \frac{1}{2}\,(u - u_{inb})\,(u + u_{inb} + 2 * u_b) \tag{3.10}$$

With a similar reasoning between points B and C :

$$h_b u_{inb} = y_c u_c \tag{3.11}$$

$$g'\,(h_b - (y_c + h_c)) = \frac{1}{2}\left(u_c^2 - u_{inb}^2\right) \tag{3.12}$$

When partial blocking occurs, unlike the super or subcritical cases, the solutions are not symmetrical over the crest, which means $\dfrac{\mathrm{d}d_1}{\mathrm{d}x}(x_{crest)} \neq 0$.
From vorticity conservation and mass conservation using that $\dfrac{\mathrm{d}h}{\mathrm{d}x}(x_{crest}) = 0$, the local Froude number over the crest F_{crest} verifies $F_{crest} = 1$.

Therefore the last equation is :

$$u_c^2 = g' y_c \tag{3.13}$$

By making equation dimensionless we obtain the following substitutions :

$$u_b^* = \frac{F - {y_c^*}^{\frac{3}{2}}}{h_b^* - 1} \tag{3.14}$$

$$u_c^* = \sqrt{y_c^*} \tag{3.15}$$

$$u_{inb}^* = \frac{{y_c^*}^{\frac{3}{2}}}{h_b} \tag{3.16}$$

We also obtain a 2×2 non-linear where h_b and y_c^* are the unknown to determine :

$$\begin{cases} 2{h_b^*}^2\,(h_b^* - 1)^2 = \left(F h_b^* - {y_c^*}^{\frac{3}{2}}\right)\left(F h_b^*\,(h_b^* - 1) + {y_c^*}^{\frac{3}{2}}\,(h_b^* - 1) + 2h_b^*\left(F - {y_c^*}^{\frac{3}{2}}\right)\right) \\ 2{h_b^*}^2\,(h_b^* - D_0) = 3{h_b^*}^2 y_c^* - {y_c^*}^3 \end{cases} \tag{3.17}$$

By solving this system numerically, it is possible to obtain the value of u_b*, h_b^*, y_c^* and u_c^* for different values of F and D_0.

In the following we will be able to compare theory and DNS for different cases i.e different (D_0, F).

3.3.2 Partial Blocking - Direct Numerical Simulations

To compare theory and numerical simulations, two points of coordinates (D_0, F) will be used, $(D_0, F) = (0.5, 0.5)$ and $(D_0, F) = (1, 0.25)$.

By solving the system for $(D_0, F) = (0.5, 0.5)$ we can obtain the different unknowns that matter and by postprocessing the DNS data we can form the following table :

$(D_0, F) = (0.5, 0.5)$	theory	DNS	relative error
h_b^*	1.2147	1.2679	4.301%
y_c^*	0.5056	0.6251	23.63%
u_b^*	0.6544	0.5814	11.15%

For $(D_0, F) = (1, 0.25)$:

$(D_0, F) = (1, 0.25)$	theory	DNS	relative error
h_b^*	1.2156	1.2379	1.832%
y_c^*	0.1444	0.2431	68.38%
u_b^*	0.9550	0.8875	1.940%

For y_c^* it is difficult to estimate its value by postprocessing the DNS data, which leads to relative errors that are important. It doesn't change the accuracy for the determination of h_b^* nor u_b^*. Indeed TURBINS [1] uses and immersed boundary method. By using this method, it is really difficult to impose free-slip condition over the obstacle. Indeed over the obstacle a no-slip condition is imposed whereas a free-slip condition should be. Therefore this leads to a biased value of the height over the crest. Physically, this phenomenon can be interpreted in the DNS by observing the boundary layer over the crest. With the implemented no-slip condition, in TURBINS, a relatively important boundary layer is present which is also affected by the Reynolds number equal to $Re = 250$. This mainly contributes to differences observed for the height over the crest in theory and DNS.

To show in each case that the steady state is reached we can plot the height and velocity over the crest y_c^* & u_c^* as functions of time and each parameter reaches an asymptote.

For $(D_0, F) = (1, 0.25)$ cf. figures 3.13 and 3.14

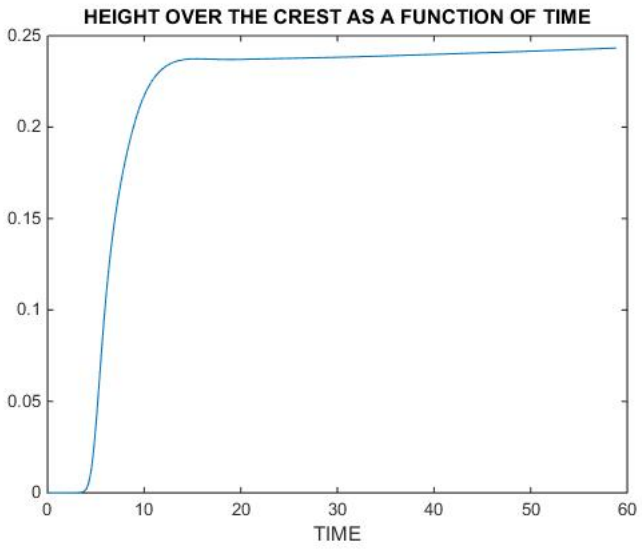

Figure 3.13: y_{c*} as a function of time

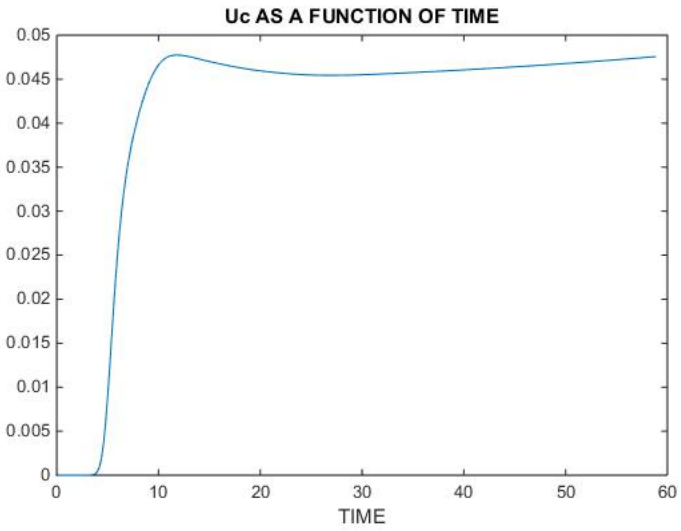

Figure 3.14: u_c^* as a function of time

Conclusion on partial blocking :

The study led in this section shows that the propagation of bores in a phenomenon which can be studied in the steady state approximation. It also underlines the consistency of the modelling in comparison with the DNS. Indeed the very good agreements for the bore height and velocity allow us to validate the results.
The following section is an interesting extension of the partial blocking. When the height over the crest reaches 0, it is possible to determine a relation with F and D_0 to determine when complete blocking occurs.

3.4 Complete Blocking

When the maximum height of the layer over the crest is equal to 0. It is possible to determine the limit of complete blocking, i.e. a relation between D_0 and F.

3.4.1 Complete Blocking and Bore Propagation - Theory

As it might not flow over the obstacle, experiments show a bore formation. This bore would propagate upstream. The bore propagation can be studied as a quasi-steady phenomenon after its formation. For the following, let's call H the channel height that would eventually tend to infinity in order to have coherence with the previous sections.

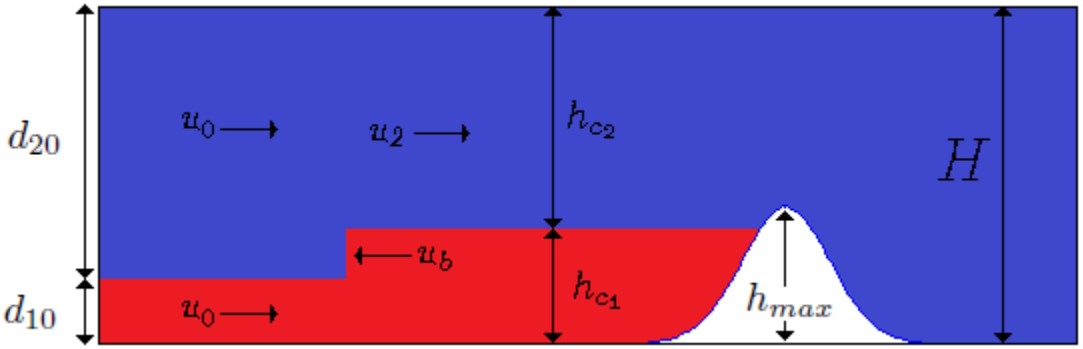

Figure 3.15: Bore propagating upstream after complete blocking by the obstacle. u_b, h_{c1} are respectively the bore velocity and its height.

IMPORTANT : Note that in this modelling h_{c_1} is similar to h_b in the previous section.
In the reference frame moving with the bore, the continuity equation in the lower layer is :

$$(u + u_b)\, d_{10} = u_b h_{c_1}$$

In the upper layer the continuity equation in the reference frame moving with the bore is :

$$(u + u_b)\, d_{20} = (u + u_b)\,(H - d_{10}) = (u_2 + u_b)\, h_{c_2} = (u_2 + u_b)\,(H - h_{c_1})$$

The vorticity equation along the interface between the lower and upper layers is :

$$g'\,(h_{c_1} - d_{10}) = u_2 \frac{(u_2 + 2u_b)}{2}$$

Complete blocking occurs when where $h_{c_1} = h(x_{crest})$. **It is also confirmed by equation 3.17 when $y_c^* = 0$, which is coherent**. By making the previous set of equations dimensionless leads to the following set of equations :

$$\begin{aligned}
&(F + u_b^*) = u_b^* D_0 \\
&(F + u_b^*)\,(H^* - 1) = (u_2^* + u_b^*)\,(H^* - D_0) \\
&D_0 - 1 = u_2^* \frac{(u_2^* + 2u_b^*)}{2}
\end{aligned}$$

From the first equation

$$u_b^* = \frac{F}{D_0 - 1}$$

then from the second

$$u_2^* = \frac{\left(F + \frac{F}{D_0 - 1}\right)(H^* - 1)}{H^* - D_0} - \frac{F}{D_0 - 1}$$

By substituting the previous variables in the third equation, the following critical curve :

$$F = (D_0 - 1)\sqrt{\frac{2(D_0 - 1)}{D_0^2\left(\frac{H^* - 1}{H^* - D_0}\right)^2 - 1}} \tag{3.18}$$

Equation 3.18 will be used to validate the theoretical results with the DNS results where the channel height will be finite, its accuracy will be discussed later.

For an infinitely deep upper layer $H \longrightarrow +\infty$, the previous critical curve reaches a limit, indeed :

$$\lim_{H^* \to \infty} F = \lim_{H^* \to \infty} \left\{ (D_0 - 1)\sqrt{\frac{2(D_0 - 1)}{D_0^2\left(\frac{H^* - 1}{H^* - D_0}\right)^2 - 1}} \right\} = (D_0 - 1)\sqrt{\frac{2}{D_0 + 1}}$$

$$F = (D_0 - 1)\sqrt{\frac{2}{D_0 + 1}} = F^*(D_0, H^*) \tag{3.19}$$

Note that equation 3.19 could have been obtained by replacing $y_c^* = 0$ in equation 3.17. This confirms the good agreement between both modellings.

The following figure 3.16 show the complete blocking region. Equation 3.18 states that for any given D_0, if the inflow Froude number F verifies $F \leq F^*(D_0, H^*)$ then complete blocking will occur.

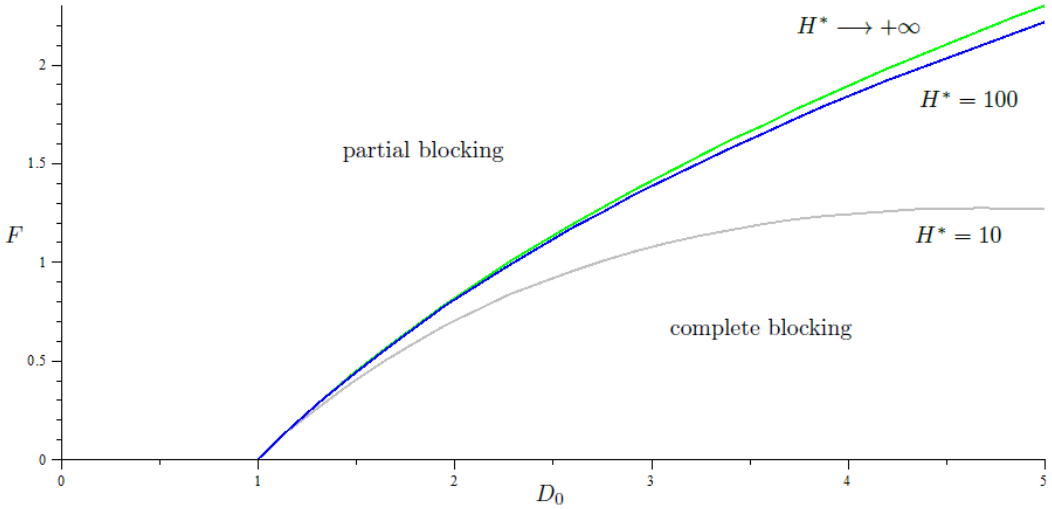

Figure 3.16: Complete blocking region under the curve of equation $F = (D_0 - 1)\sqrt{\frac{2(D_0 - 1)}{D_0^2\left(\frac{H^* - 1}{H^* - D_0}\right)^2 - 1}}$

When $(D_0, F) = (4, 1.55)$ complete blocking is expected cf. figure 3.16. Snapshots in figure 3.17 from the DNS with the previous parameters show a complete blocking and an upstream bore propagation. The bore propagation can be studied as a quasi-steady state, between in figure 3.17 when $0 \leq t^* \leq 250$, the transient regime remains. After $t^* \geq 300$ the bore has formed and propagates upstream as show in figure 3.17e where $t^* = 360$.

(a) Simulation time $t^* = 0$

(b) Simulation time $t^* = 60$

(c) Simulation time $t^* = 170$

(d) Simulation time $t^* = 250$

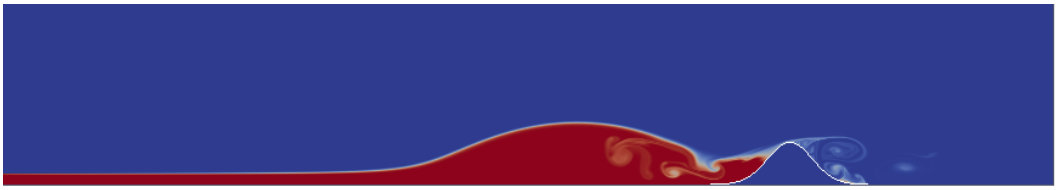

(e) Simulation time $t^* = 360$

Figure 3.17: Snapshots from the DNS for $(D_0, F) = (4, 1.55)$, the height of domain is $H^* = 80$ but for displaying convenience only the obstacle area is shown. Complete blocking is observed and the bore propagates upstream.

By post-processing the data, we are able to compute the bore velocity when quasi-steady state is reached. The procedures detects for time frames t_i and t_j $(t_i \neq t_j)$, the location $x(t_i)$ and $x(t_j)$ in the channel where the layer becomes 20% higher than the inlet height. Since the bore velocity is steady[2] we use the formula $u^*_{b_{DNS}} = \left| \dfrac{x(t_i) - x(t_j)}{t_i - t_j} \right|$.

[2]Based on differents time frames and height percentage, which also confirms the quasi-steady state.

In this case $u^*_{b_{DNS}} = 0.578$. From the first continuity equation $u^*_b = \dfrac{F}{D_0 - 1}$. Therefore, the theoretical value for the bore velocity is $u^*_{b_{th}} = 0.517$.

Hence, the relative error is $\Delta u^*_b = 100 \cdot \left| \dfrac{u^*_{b_{th}} - u^*_{b_{DNS}}}{u^*_{b_{th}}} \right| = 11.8\%$. This difference can be explained by the fact the bore, here formed, is undular, due to the maximum height of the obstacle.

3.4.2 Comparison with Houghton & Kasahara for Complete Blocking

By using the characteristics of the shallow-water equations Houghton & Kasahara [5] could obtain a limit where complete blocking would occur. Its equation is :

$$F = (D_0 - 1)\sqrt{\frac{D_0 + 1}{2D_0}} \tag{3.20}$$

In figure 3.18, the difference between the prediction using the shallow water equations and the vorticity are shown for the complete blocking.

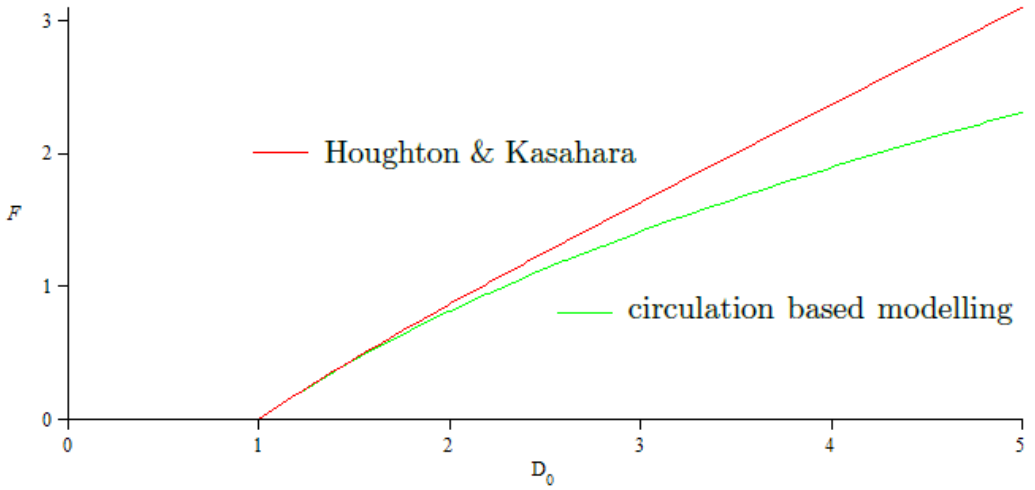

Figure 3.18: Comparison region for complete blocking. The red curve refers to equation 3.20 whereas the green refers to equation 3.19

Above the red curve, both models predict partial blocking of the fluid. Under the green curve both models predict complete blocking.The region between the two curves is narrow until $D_0 \geq 3$. To compare the two models, we choose to run a DNS for $D_0 = 4$.
For $D_0 = 4$, Houghton & Kasahara have predicted a Froude number $F_{H\&K} = 2.37$ such as if $F < F_{H\&K}$ complete blocking would occur. With the circulation based modelling, the limit Froude number F_{CBM} where complete blocking would occur is $F_{CBM} = 1.89$. Therefore the inflow Froude number will be set as $F = 2.3$ in the DNS so as to have a 20% difference with F_{CBM}. Let Φ_{inflow} be the flux of the inflow and Φ_{crest} be the flux over the crest of the obstacle. Both flow are defined as follows

$$\Phi(x^*, t^*) = \int_0^{+\infty} u(x^*, y^*, t^*) \cdot c(x^*, y^*, t^*)\, \mathrm{d}y.$$

where $c(x^*, y^*, t^*)$ is the concentration of the denser fluid and $u(x^*, y^*)$ its horizontal velocity in the DNS using TURBINS [1].

Now let us define $R_\Phi(t^*)$ the percentage of inflow flux and that goes over the crest, defined as follows :

$$R_\Phi(t^*) = 100 \cdot \frac{\Phi_{crest}}{\Phi_{inflow}} \tag{3.21}$$

When the flow is steady, $R_\Phi > 20\%$ is the criterion which will determine whether there is partial or complete blocking. By post-processing the data, we are able to plot $R_\Phi(t^*)$ in figure 3.19

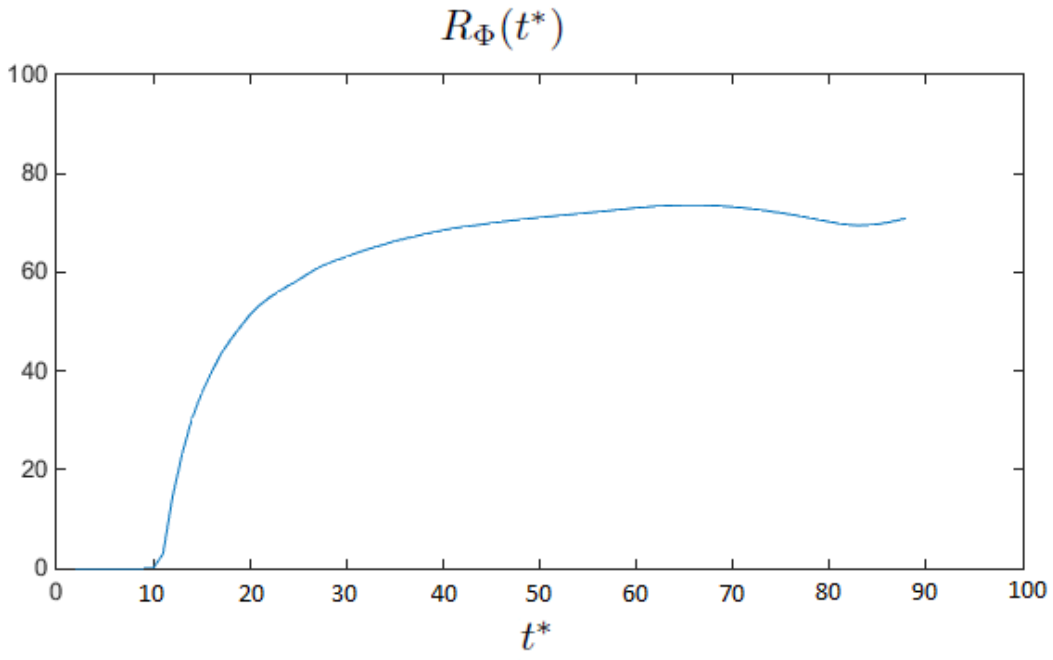

Figure 3.19: Ratio R_Φ as a function of t^*

When steady state is reached $R_\Phi(t^*) \approx 70\% > 20\%$. Hence, complete blocking, as predicted by Houghton & Kasahara, does not occur whereas the circulation based modelling for gravity current predicts complete blocking. This validate the accuracy of our model.

The previous results on the bore velocity and the accuracy of prediction for partial versus complete blocking validate the theoretical model on complete blocking.

3.5 Theoretical results on different regimes in a FINITE HEIGHT CHANNEL

Previously in section 3.2.1, theoretical results were provided when the height of the channel was assumed to be infinite. These results were provided because equation 3.6 is a third degree polynomial equation. These equations are sovable using the Cardano-Tartaglia method. Equation 3.5 is a fifth degree equation. The French mathematician Evariste Gallois proved that it is not possible to solve fifth degree (or more) equations analytically.
Even though analytical solutions can't be provided, it is still possible to obtain critical curves to differentiate the regimes.

We remind the reader that the mathematical criterion that allows one to differentiate subcritical and supercritical from partial blocking is that the LOCAL Froude number at the crest is equal to one : $F(x_c) = 1$.

The local Froude number at the crest is : $F(x_c) = \dfrac{u(x_c)}{\sqrt{g' d_1(x_c)}} = \dfrac{u^*(x_c)}{\sqrt{d_1^*(x_c)}}$

The contuinity equation at the crest is $u(x_c)d_1^*(x_c) = ud_{10}$ therefore $u^*(x_c) = \dfrac{F}{d_1^*(x_c)}$

By combining these equations $d_1^*(x_c)$ verifies : $F(x_c)\sqrt{d_1^*(x_c)} = \dfrac{F}{d_1^*(x_c)}$

So when $F(x_c) = 1$ it means that :

$$d_1^*(x_c) = F^{\frac{2}{3}} \tag{3.22}$$

Equation 3.22 also corroborates the results in subsection 3.2.2.
In order to obtain critical curves for different heights of the channel we have written an algorithm to plot the solutions that verify condition 3.22.

3.5.1 Details of the algorithm

Unlike the infinite upper layer case, it is not possible to determine an analytical critical equation like equation 3.22.

The algorithm consist in solving equation 3.5 numerically at the crest for enough points of coordinates (D_0, F) in the domain. When solution $d_1^*(x_c)$ is obtained, the algorithm must verify whether condition 3.22 is verified. If it is the case then $d_1^*(x_c)$ is stored in an array.

The following algorithm has been implemented with Matlab.

Listing 3.1: Matlab Algorithm to plot the critical curves

```
close all;
clear all;

n=1;


H=zeros(1,3); % Height of the channel 10^n times bigger than d_{10}

for i=1:3
    H(1,i)=10^(i); % Different heights of the channel : 10, 100, 1000
end
```

```
size_square_grid=1; % (In the (D_0,F) plane, we scan the whole region D_0=0 to 1
    and F=0 to 2*1

p=2;

step=size_square_grid/(10^p);
step_grid=step;     % precision to scan the region, there is a point every "step"



length=size_square_grid/step_grid;

% display(length);


F_1=zeros(1,2*length);


D_0=zeros(1,length);

for i=1:length
    D_0(1,i)=(i-1)*step;
end

for i=1:2*length
    F_1(1,i)=(i-1)*step;
end

y_c1=zeros(length,2*length);
y_c2=zeros(length,2*length);
y_c3=zeros(length,2*length);

yc_1=1.5; %initial conditions to solve numerically the following equation
yc_2=1.6;
yc_3=1.55;


x1=0;
x2=0;
x3=0;

tol=0.05;


x=zeros(1,length);
y=zeros(1,length);

for i=1:length
    y(1,i)=(i-1)*step;
end

for i=1:length
    x(1,i)=1-1.5*(y(1,i))^(2/3)+0.5*y(1,i)^2;
end


% hold on
% plot(y,x,'k');
% plot(y,-x+2,'k');
%
% break;


for k=1:3 % Different channel heights
    for j=1:2*length % For the Froude number axis
        for i=1:length % For the obstacle axis
```

```
            fun2=@(x)(  x^5 + ( D_0(1,i)-1 + 2*(D_0(1,i)-H(1,k)))*x^4 + (2*(D_0(1,
                i)-H(1,k))*(D_0(1,i)-1) + (D_0(1,i)-H(1,k))^2 )*x^3 + (0.5*F_1(1,j
                )^2*(1-(H(1,k)-1)^2) + (D_0(1,i)-H(1,k))^2*(D_0(1,i)-1))*x^2 + (
                D_0(1,i)-H(1,k))*F_1(1,j)*x +0.5*F_1(1,j)^2*(D_0(1,i)-H(1,k))^2 );
                 % Equation to solve to obtain solutions.

            if k==1
                x1=fsolve(fun2,yc_1);
                y_c1(i,j)=x1;
            elseif k==2
                x2=fsolve(fun2,yc_2);
                y_c2(i,j)=x2;
            else
                x3=fsolve(fun2,yc_3);
                y_c3(i,j)=x3;
            end

        end
    end
end

crit_1=zeros(length,2*length);

crit_2=zeros(length,2*length);

crit_3=zeros(length,2*length);

infinite_crit=zeros(length,2*length);

for i=1:length
    for j=1:2*length
        crit_1(i,j)=y_c1(i,j)*(F_1(1,j))^(-2/3)-1; % Critical curve for H=10
        crit_2(i,j)=y_c2(i,j)*(F_1(1,j))^(-2/3)-1; % Critical curve for H=100
        crit_3(i,j)=y_c3(i,j)*(F_1(1,j))^(-2/3)-1; % Critical curve for H=1000

        infinite_crit(i,j)=D_0(1,i)-1+1.5*(F_1(1,j))^(2/3)-0.5*(F_1(1,j))^(2); %
            Critical curve for H=+infty

    end
end

% Creating the arrays to plot a contour : critical curves plotting

v=[0,0];

x=zeros(1,3*length);
comp_block_1=zeros(1,3*length);
comp_block_2=zeros(1,3*length);
comp_block_3=zeros(1,3*length);
comp_block_infinite=zeros(1,3*length);


for i=1:3*length
    x(1,i)=1+(i-1)*step;
    comp_block_1(1,i)=(x(1,i)-1)*sqrt((2*(H(1,1)-x(1,i))^2)/((x(1,i)^2)*(H(1,1)-1)
        ^2 - (H(1,1)-x(1,i))^2 )); % complete blocking H=10
    comp_block_2(1,i)=(x(1,i)-1)*sqrt((2*(H(1,2)-x(1,i))^2)/((x(1,i)^2)*(H(1,2)-1)
        ^2 - (H(1,2)-x(1,i))^2 )); % complete blocking H=100
    comp_block_3(1,i)=(x(1,i)-1)*sqrt((2*(H(1,3)-x(1,i))^2)/((x(1,i)^2)*(H(1,3)-1)
        ^2 - (H(1,3)-x(1,i))^2 )); % complete blocking H=1000
    comp_block_infinite(1,i)=(x(1,i)-1)*sqrt(2/(x(1,i)+1)); % complete blocking H
        =+infty
end

% Plotting the curves

hold on
contour(D_0,F_1,crit_1',v,'k');
```

```
plot(x,comp_block_1,'k')
contour(D_0,F_1,crit_2',v,'b');
plot(x,comp_block_2,'b')
contour(D_0,F_1,crit_3',v,'g');
plot(x,comp_block_3,'g')
contour(D_0,F_1,infinite_crit',v,'r');
plot(x,comp_block_infinite,'r');
```

Hence, the critical curves are obtained in 3.20.

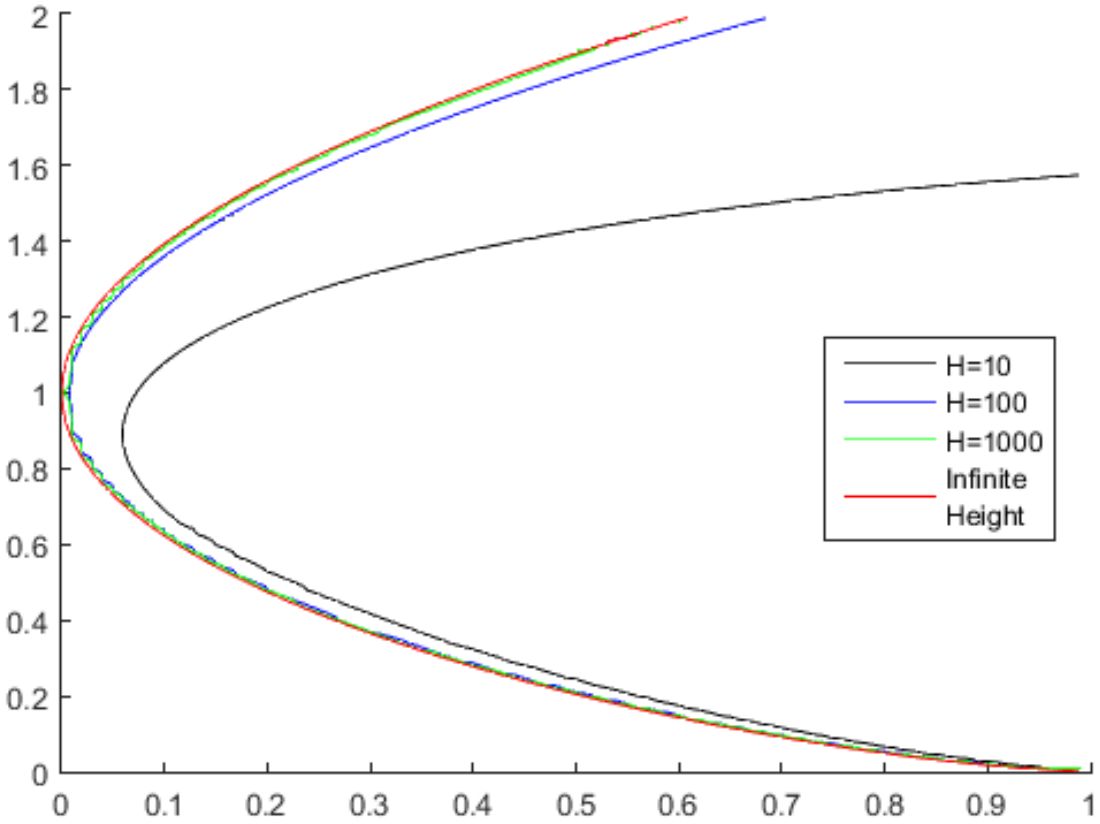

Figure 3.20: Critical Curves for different heights

3.5.2 Summary on the different flowing regimes

The following figure 3.21 sums up the four different flowing regimes for different heights. We remind the reader that these regimes are :

- Subcritical
- Supercritial
- Partially blocked
- Completely blocked

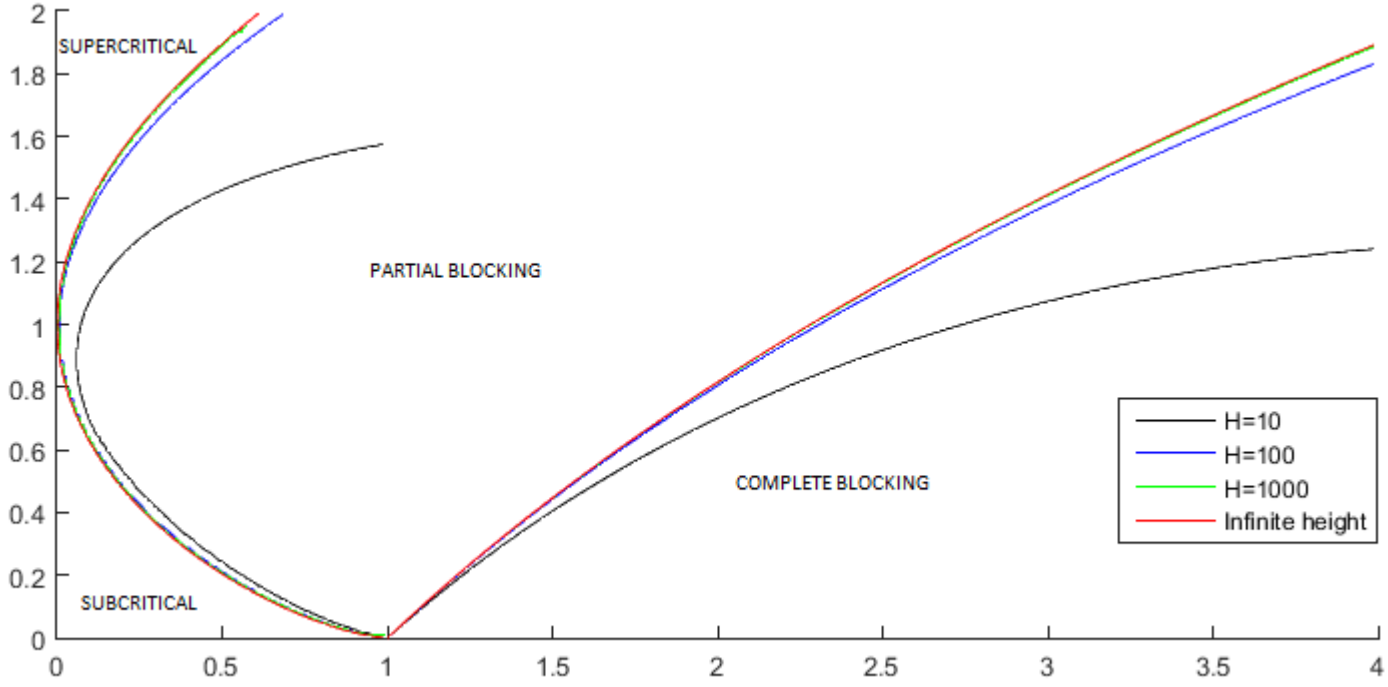

Figure 3.21: Summary of different regimes

4 Conclusion : Work and Experience

Work :

To conclude this (mainly) theoretical work, we've seen that agreements between theory and numerical simulations were close. The remaining unsolved problems, such as implementing new boundary conditions for the DNS code, are still under further investigation, though my time in UCSB is over. Indeed, the shape of the theoretical results were similar to the numerical ones.
Also in this work we can extend this application to non-Boussinesq flow and even add shear and a density gradtient.

In this report I haven't mentionned the project I was working on for one month where I had to study a lock-exchange configuration where two fluids would flow over topography. The study led to a 12×12 non-linear system which was impossible to solve analytically. We could obtain results with the Levenberg-Marquardt algorithm but it was far from satisfying. Since my time here was limited, we decided to change my research project to the study of flows over complex topography still with gravity currents.

So far, I had to use MATLAB and C, for the DNS. It helped me doing all the post-processing, initializing the DNS and creating the uniform and non-uniform grids. I also learned how to use a unix environment by using terminals and secure-shell connections. These are the tools that are essential for research in the CFD field.

Experience :

My work is far from being achieved, but so far this research internship really confirmed my will to do research in fluid mechanics in the future and go on a PhD program after my Master's degree.

During a seminar, I could meet Patrick Huerre who is the creator of the Master's degree "Fluid Dynamics : Fundamentals ans Applications" at Ecole Polytechnique. I could exchange a few words on my work and future education which was really helpful.

I really have enjoyed the time I have spent in this laboratory under the supervision of Prof. Eckart Meiburg and Mohamad Nasr-Azadani. They were tremendous tutors and mentors in this project here.
Despite an accident that led to a knee injury, I fought my way back to UCSB after a short trip in France to have treatment. Mainly, due to time limitations, leading this project to a potential article was no easy task.

Bibliography

[1] M.M. Nasr-Azadani, E. Meiburg, TURBINS: An immersed boundary, Navier−Stokes code for the simulation of gravity and turbidity currents interacting with complex topographies, Computers & Fluids 45 (2011) 1428 (2010)

[2] von Karman, T. 1940 The engineer grapples with nonlinear problems. Bulletin of the American Mathematical Society 46 (8), 615683.

[3] Benjamin, T. B. 1968 Gravity currents and related phenomena. Journal of Fluid Mechanics, **31** (2), 209248.

[4] R.R. Long, Some Aspects of the Flow of Stratified Fluids, A QUARTESLY JOURNAL OF GEOPHYSICS, vol. 6, no. 2, 1954, pp. 97 to 115.

[5] D D. Houghton and A. Kasahara, Nonlinear shallow fluid flow over an isolated ridge, NCAR Manuscript, no. 259a, 1967

[6] M.M. Nasr-Azadani, E. Meiburg, Gravity currents propagating into shear, under review ,2015